https://doi.org/10.31399/asm.cp.am-epri-2004p0403

Proceedings from the Fourth International Conference on Advances in Materials Technology
for Fossil Power Plants, October 25–28, 2004, Hilton Head Island, South Carolina.

Characterization of Multi-Scale Structures for a Creep-Fatigued Ferritic Heat-Resisting Steel

M. Hayakawa, K. Yamaguchi, M. Kimura, K. Kobayashi
Materials Information Technology Station, National Institute for Materials Science
1-2-1 Sengen, Tsukuba, Ibaraki, Japan 3050047

Abstract

Microstructural analyses by FE-SEM and TEM were performed on a ferritic heat-resisting steel that contained 12mass% chromium and 2mass% tungsten to characterize its multi-scale structure, consisting of prior austenite grains, packets, blocks, subgrains and precipitates. The size distributions of the block, subgrains and precipitates were quantitatively evaluated before and after a creep-fatigue test to relate them to their creep-fatigue property. Our results showed that the occupancy of precipitates on prior austenite grain boundaries increased markedly and subgrains became coarse during the creep-fatigue test, while block size did not change. It is suggested that the growth of grain boundary precipitates and coarse subgrains plays an important role in the intergranular fracture mechanism caused by creep-fatigue.

1. Introduction

Optical microscopic observations have revealed that ferritic 12Cr-2W steel has a tempered martensite structure (Fig. 1(a)) [(1)]. As shown in the schematic diagram in Fig. 1(b), the multi-scale structure consist, in descending order of size, of prior austenite (γ) grains, packets, blocks and subgrains. Several studies have been conducted on the multi-scale structure of ferritic steels, but most other studies have focused on changes in the distribution of precipitates and on transmission electron microscopic (TEM) observations.

The authors characterize microstructures of the ferritic heat-resisting steel. Electropolished surfaces of the ferritic 12Cr-2W steel were observed under a field emission-type scanning electron microscope (FE-SEM), and thin films of these specimens were observed under a TEM. FE-SEM, which has a resolution one order higher than that of an ordinary SEM.

In this study, precipitates, blocks and subgrains of ferritic heat-resisting 12Cr-2W steel were quantified based on the microstructural observation. In particular, we focused on differences in the distributions of precipitates before and after creep-fatigue testing. This study also proposes a

simple method for quantifying precipitate distribution, which reflects changes in the microstructure caused by creep-fatigue.

2. Experimental procedure

2.1 Materials

The specimen was 12Cr-2W steel, excised from a thick-walled pipe (ASTM-SA355-P122) that had been processed for use as a main steam pipe in a fossil fuel power plant. The chemical compositions and thermal treatments are shown in Table 1. The material had been normalized at 1323 K for 3.6 ks and cooled in air. It was then tempered at 1053 K for 21.6 ks. Most prior γ grains were approximately 150 to 200 μm in diameter.

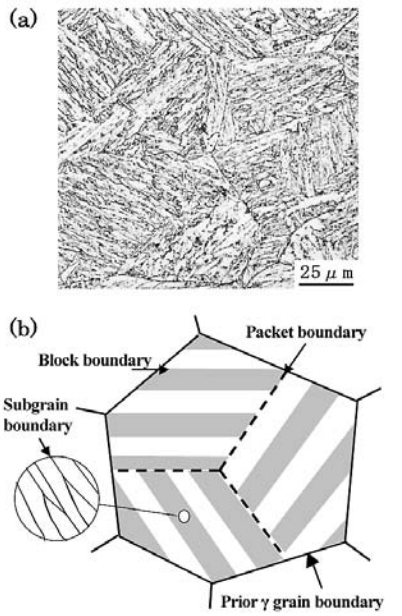

Fig. 1 Optical image and schematic illustration of the microstructure factors within a prior austenite (γ) grain are shown in (a) and (b), respectively.

The data on tensile tests, creep rupture tests and creep-fatigue tests are reported in previous papers [1]. The creep fatigue tests were conducted at 923 K. Trapezoidal waves were used to apply strain. The total stain range of the waves was 1.0%. The duration of 1.0% strain was 10.8 ks. The transition strain rate was 5×10^{-4} /s. The resultant cycles for creep-fatigue rupture (creep-fatigue life) were 309 cycles (total duration: 3349 ks). Fractures originated at prior γ grain boundaries.

2.2 Specimen preparation

Thin sections 7 mm in length, 5 mm in width and 1 mm in thickness were excised before and after the creep-fatigue test (after fracture) along the load direction of the parallel gauge. The surfaces were buff-polished using diamond particles 1 μm in diameter, and were finished by electropolishing. Electrolyte (1000 cm^3) was prepared by mixing 80 cm^3 perchloric acid, 700 cm^3 ethanol, 100 cm^3 butoxy-ethanol and 120 cm^3 distilled water. A voltage of 40 V was applied for 10 s. Since the rate of electropolishing depends on precipitate phase and crystal orientation,

Table 1 Chemical composition and thermal processing are shown in (a) and (b), respectively.

(a) Chemical composition (mass%) of the material used.

Material	Form	C	Si	Mn	Cu	Ni	Cr	W	Mo	V	Nb	N	Fe
12Cr-2W	Pipe	0.14	0.26	0.65	0.74	0.4	11.03	1.95	0.29	0.2	0.07	0.06	Bal.

(b) Thermal processing of the material used.

Material	Form	Normalizing		Tempering	
12Cr-2W	Pipe	1323 K, 3.6 ks	Air cooled	1053 K, 21.6 ks	Air cooled

this treatment causes slight unevenness to be formed on the surface [2, 3]. FE-SEM can detect minute changes in level that identify the microstructure.

3. Results ans discussion

3.1 Tempered martensite microstructure

Fig. 2 shows FE-SEM images before the creep-fatigue test. The black and white contrast in the images shows the level differences on the electropolished surface. These differences in level are attributable to differences in the rate of electropolishing, which in turn depend on the crystal orientation and phase at the surface. The smallest crystal phase that has high misorientation angle boundary is a block [4, 5]. The black and white contrast identifies blocks. Packets are where blocks are arranged in parallel alignment. Prior γ grains contain several packets. Prior γ grain boundaries are longer than the packet boundaries and can be separately identified.

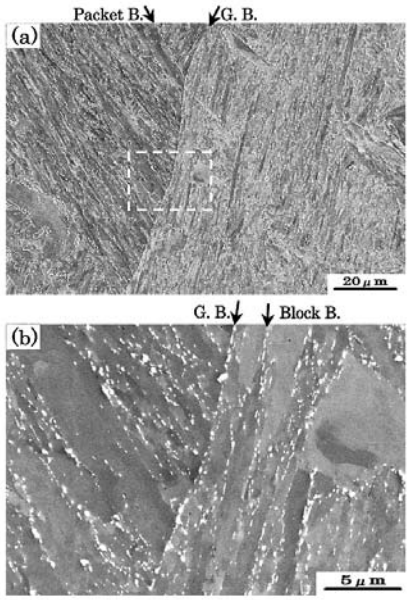

Fig.2 FE-SEM images of the specimen before the creep-fatigue testing. The larger magnification image of the area shown with white doted lines in (a) is shown in (b).

Precipitate particles are shown as white spots extruding from the base metal. These were dense on high misorientation angle boundaries such as block boundaries, packet boundaries and prior γ grain boundaries.

Fig. 3 shows FE-SEM images of the electropolished surface after the creep-fatigue test. As before the test, blocks, packets and prior γ grains are observed on the martensite base. The precipitate particles are larger than those before the test. Precipitates on the boundaries are also denser. On prior γ grain boundaries, particularly coarse precipitations are observed where precipitates were dense and formed a film-like cover.

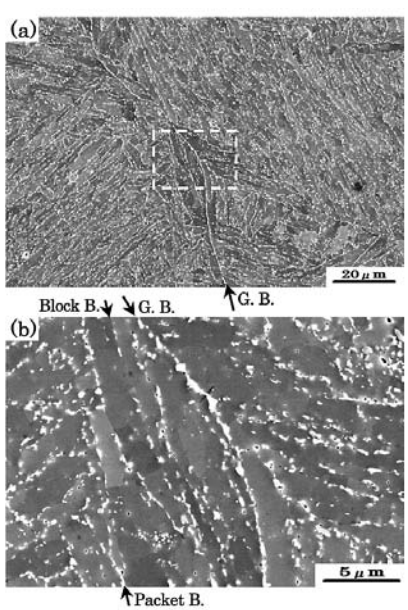

Fig.3 FE-SEM images of the specimen after the creep-fatigue testing.

Figs. 4(a) and 4(b), respectively, show TEM images of microstructures before and after the test. Similarly contrasted regions can be seen in the images. These regions are subgrains: crystal units with a low misorientation angle boundary. In a TEM image, to identify a block, which is a group of subgrains, the

crystal orientations of every subgrain must be identified. Subgrains after the creep-fatigue test are notably coarser than those before the test. In Fig. 4(a), the dislocation density within subgrains was high, and dislocations were difficult to distinguish from precipitates. On the other hand, in Fig. 4(b), the dislocation density was low, allowing precipitates to be easily distinguished from dislocations. In spite of this, separate identification of dislocations and precipitates was difficult near boundaries.

These observations show that FE-SEM and TEM can be combined to quantitatively analyze the multi-scale structure of 12Cr-2W steel, which comprises structural factors of varying sizes. FE-SEM images are suitable for estimating the sizes of precipitate particles and blocks. TEM images are suitable for estimating the size of subgrains.

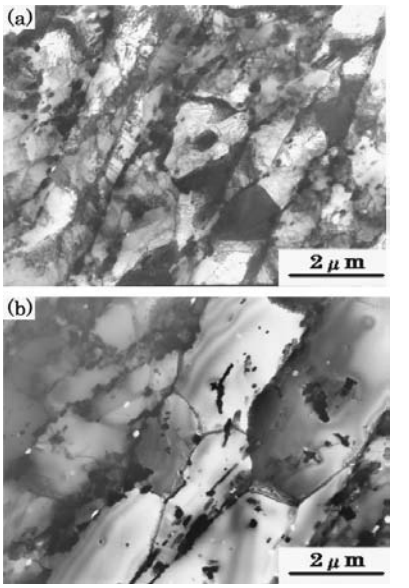

Fig4 TEM images of the specimen before and after the creep-fatigue testing in (a) and (b), respectively.

3.2 Changes in microstructure caused by creep-fatigue

3.2.1 Distribution of precipitates

Fractures originated at prior γ grain boundaries during the creep-fatigue test. Precipitates on boundaries have been shown to play important roles in intergranular fracture mechanisms of tempered martensitic steels [3, 6]. For this reason, the authors quantified precipitate distribution separately for the entire microstructure (intragranular) and prior γ grain boundaries (intergranular).

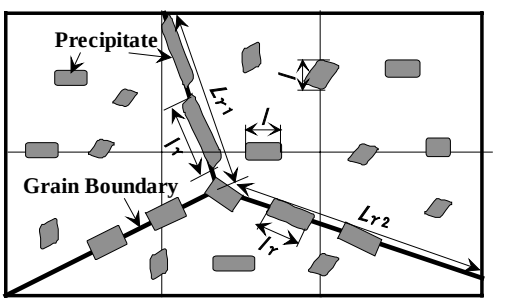

Fig.5 Schematic drawing of the intra- and inter-granular precipitates.

Measuring the sizes of all precipitate particles on FE-SEM images is unrealistic, since they are too numerous. The size of precipitates on the entire microstructure was estimated by applying the cutting method used to determine nominal grain size. As schematically shown in Fig. 5, each FE-SEM image (×5000) was divided into six equal sections by drawing two vertical lines and one horizontal line. (The length of each segment line is L.) The sum of the length of precipitates on the lines (referred to here as the "nominal precipitate particle length l" for convenience) and the occupancy on the lines (referred to here as the "mean volumetric occupancy f" for convenience) were calculated as $f = \Sigma(l/L)\times 100(\%)$. If the segment lines are long enough compared to precipitate size, f reflects the mean volumetric occupancy of the precipitate.

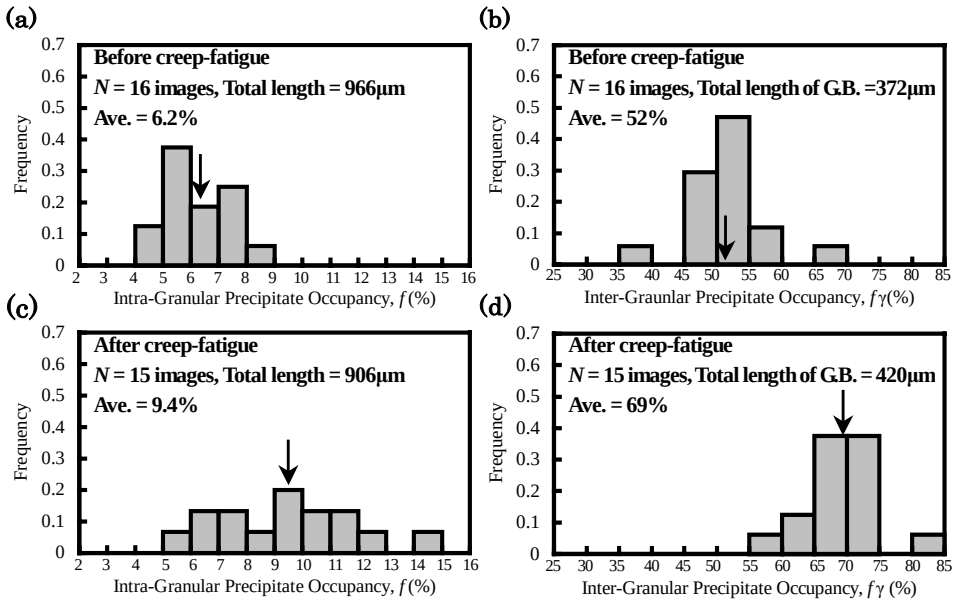

Fig.6 The frequency of the intra- or inter-granular precipitate occupancy of each of FE-SEM image (x5000) before and after the creep-fatigue testing, respectively.

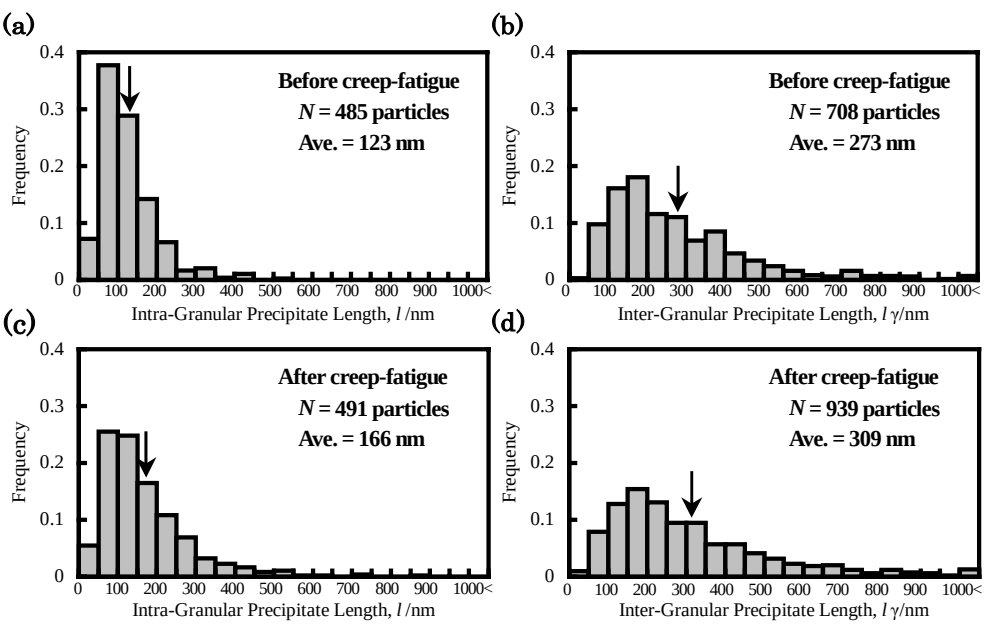

Fig.7 The frequency of the intra- or inter-granular precipitate length before and after the creep-fatigue testing, respectively.

The occupancy of prior γ grain boundary by precipitates (referred to here as "grain-boundary occupancy") $f_\gamma = \sum(l_\gamma / L_\gamma) \times 100(\%)$ was determined for each visual field of FE-SEM image

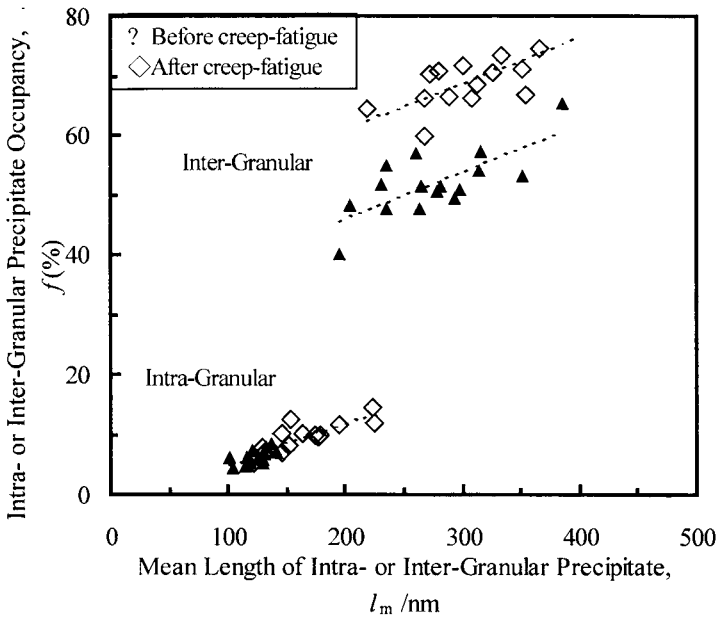

Fig.8 The relationship between precipitate occupancy and mean length of the intra- or inter-granular precipitate of each of FE-SEM image (x5000) before and after the creep-fatigue testing, respectively.

(×5000), where l_γ is the length of a precipitate particle along the direction of the prior γ grain boundary (referred to here as the "grain-boundary precipitate length" for convenience) and L_γ is the length of the grain boundary. The grain boundary occupancy is also the boundary volumetric occupancy, assuming the width of precipitates on the grain boundaries to be uniform.

Fig. 6 shows histograms of mean volumetric occupancy and grain-boundary occupancy for the specimens before and after the creep-fatigue test. The values were determined for each FE-SEM visual field (×5000). The mean volumetric occupancy for all visual fields before the test was 6.6%. The mean grain-boundary occupancy was 52%. On the other hand, in the fractured specimens, the mean volumetric occupancy for all visual fields was 9.0%. The mean grain-boundary occupancy was 69%.

Fig. 7 shows histograms of nominal precipitate particle length l and grain-boundary precipitate particle length l_γ of the specimens before and after the creep-fatigue test. Before the test, the mean nominal precipitate length was 123 nm, and the mean grain-boundary precipitate length was 273 nm. In the fractured specimens, or after the test, the mean nominal precipitate length was 166 nm. The mean grain-boundary precipitate length was 309 nm.

Based on the results, the relationship between volumetric occupancy and precipitate length was analyzed. Fig. 8 is a plot of mean volumetric occupancy and grain-boundary (volumetric) occupancy against mean nominal precipitate length and grain-boundary precipitate length, respectively. The Figure shows the results before and after the creep-fatigue test. The relationship between mean volumetric occupancy and nominal precipitate length shows the condition of the entire specimen. The relationship was linear before and after the test, showing

that they were mutually proportional. The relationship between the grain-boundary occupancy and grain-boundary precipitate length was also linear, showing that they were similarly mutually proportional. However, in the fractured specimens, the increase in grain-boundary occupancy was greater than the increase in precipitate length.

Our results show that changes in precipitate distribution are more notable on prior γ grain boundaries than in grains. Therefore, grain-boundary occupancy can be used as an index of damage to the microstructure by creep-fracture that originates at prior γ grain boundaries.

3.2.2 Blocks

Whether the mechanical strength of tempered martensitic steels is determined by blocks has been much discussed [5, 7, 8]. The block widths were measured before and after the creep-fatigue test from FE-SEM images, and the distributions of the measurements were compared. High misorientation angle boundaries, such as prior γ grains, packets and block boundaries, act as preferential sites for precipitation, and are thus densely covered by precipitates. Thus, the blocks can be identified from the contrast with the martensite base and from the distribution of precipitates.

Fig. 9 shows distributions of block widths before and after the test. The mean block widths before and after the test were 1.58 μm and 1.62 μm, respectively, showing similar values. The creep-fatigue test up to rupture did not cause many changes in the size of the block structure (including the packet and prior γ grains, which are structural constituents larger than the block scale).

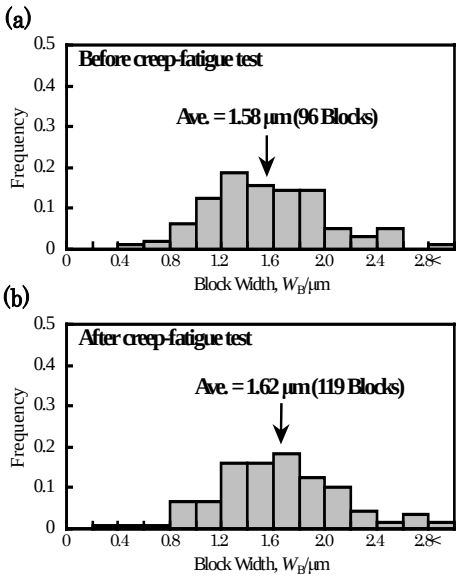

Fig.9 The frequency of the block width measured in several FE-SEM images before and after the creep-fatigue testing in (a) and (b), respectively.

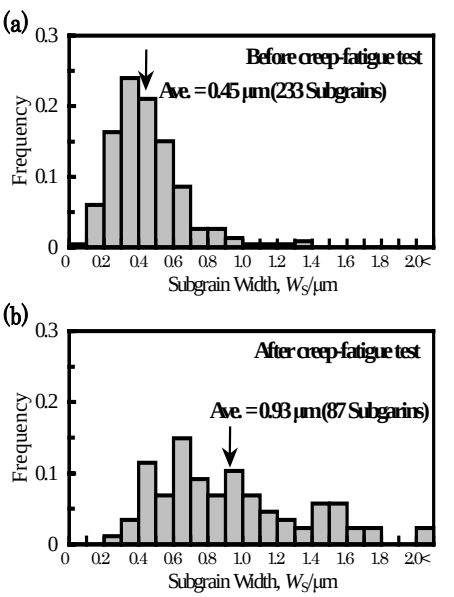

Fig.10 The frequency of the subgrain width measured in four TEM images before and after the creep-fatigue testing in (a) and (b), respectively.

3.2.3 Subgrains

As clearly shown in the TEM images in Fig. 4, the subgrain structures differed notably between before and after the creep-fatigue test. Fig. 10 shows the distributions of subgrain widths (widths of elliptic subgrains or diameters of equiaxial subgrains) that were measured in four fields of TEM images for each before and after the test (same magnification as in Fig. 4). The mean subgrain width before the test was 0.45 μm and that after the test was 0.93 μm, showing the subgrains to have almost doubled in size up to creep-fatigue rupture. After the test, the subgrains showed greater deviation in size, with coarse subgrains larger than 2 μm in width being formed. In consideration of the facts that the mean subgrain width was smaller than the mean block width and that the block width did not change during the test, it is unlikely that subgrains grow to exceed the size of the block b oundaries. Block boundaries are high misorientation angle boundaries and are densely covered by precipitates, which may act as barriers to the growth of subgrains. Therefore, the coarse subgrains of over 2 μm in width are likely to have formed within relatively large blocks over 2 μm in size.

3.3 Relationship between microstructure and creep-fatigue property

Table 2 separately summarizes the measurements of microstructural constituents before and after the creep-fatigue test for within the prior γ grains and on the prior γ grain boundaries. During the process of creep-fatigue rupture, the block structure showed no changes, whereas marked differences were observed in the precipitate and subgrain structures.

The density of precipitates, especially the occupancy of prior γ grain boundaries, increased. The main precipitates of high-chromium-tungsten ferritic steel are thought to be $Cr_{23}C_6$ and Fe_2W (Laves phase) [9]. However, it is difficult to identify precipitates on grain boundaries from FE-SEM images. If the creep-fatigue fractures originated on grain boundaries, increases in precipitate density (or occupancy) may have weakened the bonding force between grains. If this is the case, changes in the occupancy of precipitates on grain boundaries during the creep-fatigue rupture test can be used as a new index to show sensitivity to grain-boundary fracture.

On the other hand, subgrains are structural factors within prior γ grains. When there were coarse blocks near prior γ grain boundaries, local deformations were concentrated near the boundaries [7]. During creep tests, recovery near the prior γ grain boundaries progressed prior to recovery in other regions, and grown coarse subgrains are considered to accelerate grain boundary rupture [10]. Therefore, if coarse subgrains over 2 μm in width are frequently formed near prior γ grain boundaries during creep-fatigue tests, they are likely to be implicated in grain

Table 2 Summary of the microstructure factors before and after the creep-fatigue testing.

	Inner prior austenite grain				: Prior austenite grain boundary		
	Block Width W_B/μm	Subgrain Width W_S/μm	Precipitate length l/nm	Precipitate occupancy f(%)	:	Precipitate length l_γ/nm	Precipitate occupancy f_γ (%)
(a)Before	1.58	0.45	123	6.2	:	273	52
(b)After	1.62	0.93	166	9.4	:	309	69

boundary fractures. Non-uniform changes in precipitate and subgrain distributions appear to be related to creep-fatigue fractures originating at grain boundaries. However, the positional relationship between these coarse subgrains and prior γ grain boundaries could not be determined due to the small visual field of the TEM images. One of our future studies is to identify the distribution of coarse subgrains in multi-scale structures.

4. Conclusions

(1) An estimation method was proposed to show non-uniform changes in the distribution of precipitates during creep-fatigue tests. The method showed that a) occupancy of prior γ grain boundaries by precipitates was high in ruptured specimens, and b) changes in distribution of precipitates on the boundaries were non-uniform compared to those in the entire microstructure.

(2) The creep-fatigue test up to rupture caused no changes in block size.

(3) The creep-fatigue test caused coarse subgrains with widths of over 2 μm to be formed, widening the distribution of subgrain sizes.

(4) Non-uniform changes in precipitate and subgrain distribution, which were observed locally compared to those in the entire microstructure, were suggested to be related to creep-fatigue fractures that originate at grain boundaries.

References

1. M. Kimura, K. Kobayashi and K. Yamaguchi: Mater. Sci. Res. Inter. **9** (2003) 50-54.
2. M. Hayakawa, S. Matsuoka and K. Tsuzaki: Mater. Trans. **43** (2002) 1758-1766.
3. M. Hayakawa, S. Matsuoka, K. Tsuzaki, H. Hanada and M. Sugisaki: Scr. Mater. **47** (2003) 655-661.
4. A. R. Marder and G. Krauss: Trans. ASM **60** (1967) 651-660.
5. T. Maki, K. Tsuzaki and I. Tamura: Trans. ISIJ **20** (1980) 207-214.
6. G. Krauss and C. J. McMahon Jr.: *Martensite*, eds. by G. B. Olson and W. S. Owen, New York: ASM International, 1992, pp. 295-321.
7. M. Hayakawa, S. Matsuoka and Y. Furuya: Mater. Lett. **57** (2003) 3037-3042.
8. H. Hirukawa, S. Matsuoka, K. Miyahara and Y. Furuya: Mater. Lett. **58** (2004) 321-325.
9. F. Abe, H. Araki and T. Noda: Metall. Trans. A **22A** (1991) 2225-2235.
10. K . Kimura, T. Matsuo, M. Kikuchi and R. Tanaka: Tetsu-to-Hagane **72** (1986) 474.